Nonlinear Analysis: Real World Applications 50 (2019) 342–364

Contents lists available at ScienceDirect

Nonlinear Analysis: Real World Applications

www.elsevier.com/locate/nonrwa

Vibrations of a Gao beam subjected to a moving mass

B. Dyniewicz [a], C.I. Bajer [a], K.L. Kuttler [b], M. Shillor [c,*]

[a] *Institute of Fundamental Technological Research, Polish Academy of Sciences, Pawińskiego 5b, 02-106 Warszawa, Poland*
[b] *Retired*
[c] *Department of Mathematics and Statistics, Oakland University, Rochester, MI 48309, USA*

ARTICLE INFO

Article history:
Received 14 December 2018
Received in revised form 14 May 2019
Accepted 15 May 2019
Available online xxxx

Keywords:
Dynamic vibrations
Buckling of a Gao beam
Moving point-load

ABSTRACT

This paper models, analyzes and simulates the vibrations of a nonlinear Gao beam that is subjected to a moving mass or a massless point-force. Such problems arise naturally in transportation systems such as trains or trams. The dynamics of the system as the mass or the force move on the beam are investigated numerically in the cases when the vibrations are about a buckled state, and in the cases when the mass is positive or vanishes. The simulations are compared to those of the Euler–Bernoulli linear beam and the differences are highlighted. It is seen that the linear beam may be used only when the loads are small, while the Gao beam allows for moderate loads. The simulations are based on a time-marching finite elements algorithm for the model that has been developed and implemented. The results of representative and interesting computer simulations are depicted. The existence of weak solutions of the model is established using a variational formulation of the problem and results about variational set-inclusions.

1. Introduction

The motion of a point load on a metallic beam is of considerable importance in many applications, especially in railway systems, but also in construction (e.g., cranes) and many others. This explains the rich and extensive scientific literature on the subject, see, e.g., [1,2] or [3]. Their fundamental importance in railway transportation lies in the fact that the dynamic vibrations of the rail systems, when trains or trams travel them, may cause unwanted damage to the supports and cause unwanted noise [4] and dynamic wear. Indeed, there is a need for accurate prediction of such vibrations and their effects on the reliability of the system it is important to understand and possibly control the noise generated by such processes.

This work is a contribution to the field and deals with accurate predictions of the system vibrations. It is a continuation of the study of the dynamic of systems that include the so-called 'Gao beam,' the equation

* Corresponding author.
E-mail addresses: bdynie@ippt.gov.pl (B. Dyniewicz), cbajer@ippt.gov.pl (C.I. Bajer), klkuttler@gmath.com (K.L. Kuttler), shillor@oakland.edu (M. Shillor).

https://doi.org/10.1016/j.nonrwa.2019.05.007

of motion of which allows for vibrations about buckled states, [5–7]. We model, analyze and investigate computationally the horizontal motion of a vertical point-load that has either mass (inertial) or is massless, on a metallic rail and the resulting oscillations of the system. Our study is motivated, in part, by the previous works on railway systems, see, e.g., [8,9] and the references therein. This subject has been extensively treated in many publications, however, the assumptions and mechanical models used by various researchers were incomplete and sometimes too simplistic. First, the track was subjected to a set of massless forces applied with more or less complex oscillators. Moreover, the dynamic properties and responses were not affected by the additional inertia of the wheel-sets, which are invariably present in transportation applications. Indeed, their mass is about 750 kg per wheel and, hence, cannot be neglected, see e.g., [10,11]. Second, the axial forces in the rails were too simplistic. Third, the temperature variations in the rails can be more than 40 °C during a day and more than 70 °C during a year. Such variations in the temperature cause significant changes in the stresses in the system and the mathematical models for the structures must take these processes into account. This work addresses the first and second issues, while the inclusion of thermal effects will be studied in the future.

Models for a Gao beam were derived and simulated in [5,12–14] (see also the references therein). They were investigated mathematically and computationally in [6,7,15–19]. Basic mathematical analysis of the model can be found in [6] where the solutions existence was established and problems that involve contact studied. The dynamic contact of a Gao beam with a reactive or rigid foundation was described in [19]. The case of vibrations of a Gao beam whose end is restricted to move between two rigid or reactive stops was studied in [15], and the analysis of the problem of two coupled Gao beams connected via a joint with a gap can be found in [18]. Vibration characteristic of contacting one-dimensional structures with a Gao beam were conducted in [17], where the model, existence of weak solutions, and computer simulations can be found. Finally, an interesting problem was studied in [7] where the growth of a crack in a Gao beam was analyzed and simulated. Concerning models for contact, we refer to [20] and the many references therein.

The model we construct for the dynamics of a force that acts on a point-mass or massless that is moving on a straight rail, assumed to be of the Gao type, results in an unusual coupled system of a nonlinear beam equation and an ordinary differential equation for the motion of the mass. The system is given in (2.1) and (2.6). For the sake of generality, we assume that the horizontal motion of the point-mass and the load acting on it are time dependent, possibly periodic. We use our basic result in [21] to prove that the system, which has an unusual form, has a weak solution.

Next, we develop a 2D space–time FEM numerical algorithm for the model. However, in the simulations, for the sake of simplicity, we assume that the point-mass is moving with a constant velocity and the load on it is constant. Even this slightly simpler setting still contains most of the interest in the problem. Allowing for periodic oscillations of the mass and variable loads are of interest, and will be studied in the sequel. In the simulations algorithm, the FEM method allows us to derive characteristic matrices that deal well with the nonlinear terms in the differential equation. The numerical examples show the efficiency of the computational method. In particular, they clearly exhibit the difference between the classical linear Euler–Bernoulli beam and the Gao beam model. The nonlinear terms significantly change the dynamic response and affect the interplay between the stiffness of the beam and the frequency of the vibrations. The computer simulations study the influence of the compressive force on the dynamic response of the Gao beam to a massless or inertial load. The system's sensitivity to the horizontal traction force, load component and to its velocity are presented. Moreover, we use repeating crossing of the load over the whole span of the beam to exhibit the difference in displacements as a function of time. We also investigate the advantages of the Gao model as compared with the commonly used Euler–Bernoulli model.

We now describe the remaining sections of this paper. The 'classical formulation' of the model is presented in Section 2. We choose the material constitutive law to be viscoelastic of the Gao type. To model the moving point-mass we use the Dirac distribution and the associated Renaudot condition. This leads to a coupled

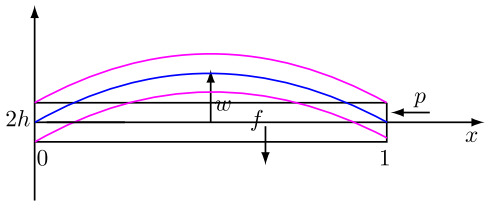

Fig. 1. The Gao beam without a moving load; $w(x,t)$ denotes the displacement of the central axis. The lengths are scaled so that $L = 1$.

system that consists of the dynamic Gao beam equation with the point-mass added, and the Renaudot condition at the position of the mass. For the sake of generality, we allow the force that acts on the mass and the velocity of the mass to be time-dependent. The existence of a weak or variational solution to the model is presented in Section 3, based on an interesting version of a theorem in [21]. A numerical space–time FEM scheme for the problem is constructed in Section 4. The convergence of the algorithm remains an open question. Moreover, as was noted above, we assume in the simulations that the point-load and the velocity of the mass are time-independent, and the beam is elastic. The implementation of the algorithm and six numerical simulations of the problem are depicted in Section 5. The paper concludes in Section 6 with some open questions.

2. The model

We construct a model for the motion of a point-mass on a rail that is assumed to be a Gao beam, which is extension of the one in [22]. The setting is described in Fig. 1, without the moving mass and in Fig. 2 where a point-load P acts on the moving mass m. Moreover, a horizontal traction acts on the right end of the beam, and when it is sufficiently large it may cause vibrations about a buckled state, which makes the motions much more complex and interesting.

The extension of the model in [22] consists of careful considerations of the coupling between the motion of the mass and the vibrations of the beam. The setting is as follows, where all the lengths are scaled with the beams's length L. The beam's centerline is $[0,1]$; the (scaled) thickness is $2h$, and $w(x,t)$ denotes the scaled transverse displacement of the central axis. A derivation of the Gao beam model can be found in [5,13], and related models can be found in the references in the introduction. The beam is clamped at both ends ($x = 0, 1$) and a horizontal traction p, which may depend on time, acts at the end $x = 1$. When the traction is tensile ($p < 0$) the beam behaves essentially as an Euler–Bernoulli beam. However, when the traction is compressive and sufficiently large, say $p > p_* > 0$, for some threshold p_*, the beam exhibits two buckled states that are stable and the zero steady state that is unstable. This allows for vibrations about each one of the two buckled states. For the sake of generality, we allow the traction $p = p(t)$ to be time dependent and possibly periodic.

The Gao beam is described by the dynamic equation

$$\rho w_{tt} + k w_{xxxx} + \gamma w_{txxxx} + (\overline{\nu} p - a w_x^2) w_{xx} = \rho f,$$

where here and below, the subscripts x and t denote partial derivatives, f is the density of applied distributed force (per unit mass), ρ is the material density (mass per unit cross-sectional area), $k = 2h^3 E_Y/3(1-\tilde{\nu}^2)$, $\overline{\nu} = (1+\tilde{\nu})$, and $a = 3h\, E_Y$; $\tilde{\nu}$ and E_Y are the Poisson ratio and the Young modulus, respectively. Also, for mathematical reasons, we added a viscosity term γw_{txxxx}, with viscosity coefficient $\gamma > 0$, assumed to be small.

Our interest lies in the lateral motion of a concentrated load $P = P(t)$, which may vary with time, that is applied to a moving mass m that is at position $\xi(t)$ and has horizontal velocity $\dot{\xi}(t) = v(t)$, that is caused

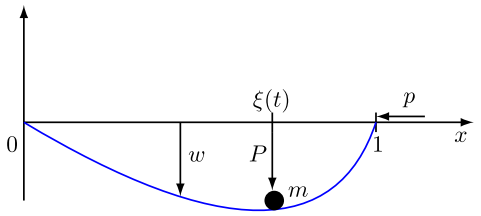

Fig. 2. The Gao beam with a moving load $P(t)$ that acts on m at $x = \xi(t)$.

by a horizontal applied force $f^*(t)$. Here and below, a dot above a symbol represents the time derivative. Moreover, unlike our previous work [22], here the traction at $x = 1$ does not vanish, $p > 0$, and is large enough to cause buckling.

To obtain the modifications of the model caused by the moving mass, which leads to non-constant density, we use Newton's law of motion in its general form, i.e.,

$$\frac{\mathrm{d}}{\mathrm{d}t}(MV) = F,$$

where F is the total force, M is a variable mass and V is its velocity, so that MV is the system momentum.

A careful examination of the forces and the rate of change of the momentum shows that the term ρw_{tt} has to be replaced by

$$\rho w_{tt} + m\delta(x - \xi(t))w_{tt} + m\delta'(x - \xi(t))v(t)w_t.$$

Here, $\delta(x)$ is the Dirac function (actually a distribution centered at the origin) and $\delta'(x)$ is its distributional derivative. Next, we represent the load on the mass by $\delta(x - \xi(t))P(t)$. Finally, the equation of horizontal motion of the mass, in absence of friction, is just

$$m\ddot{\xi} = f^*.$$

The 'classical formulation' of the *dynamic model for a viscoelastic beam with finite deformations and a moving point-load* is as follows.

Problem 2.1. Given the external force $f = f(x,t)$, the horizontal force $f^*(t)$, the traction $p = p(t)$, and the point load $P = P(t)$; find the displacement field $w = w(x,t)$, for $x \in (0,1)$ and the position of the mass $\xi(t)$, $t \in [0,T]$, such that

$$\begin{aligned}
\rho w_{tt} + m\delta(x-\xi)w_{tt}(\xi,t) + m\delta'(x-\xi(t))v(t)w_t + kw_{xxxx} + \gamma w_{txxxx} \\
-(aw_x^2 - \overline{\nu}p)w_{xx} = \rho f + \delta(x-\xi)P, && (2.1)\\
m\ddot{\xi} = f^*, && (2.2)\\
w(0,t) = w_x(0,t) = 0, && (2.3)\\
w(L,t) = w_x(L,t) = 0, && (2.4)\\
w(x,0) = w_0(x), \quad w_t(x,0) = v_0(x), \quad \xi(0) = \xi_0, \quad v(0) = \xi_{00}. && (2.5)
\end{aligned}$$

The initial data $w_0(x), v_0(t), \xi_0$ and ξ_{00} are given and have the appropriate smoothness. We note here that

$$\xi(t) = \xi_0 + \int_0^t \dot{\xi}(\tau)\,\mathrm{d}\tau.$$

This, in particular, implies that the model ceases to make sense beyond the time T^* when either $\xi(T^*) = 0$ or $\xi(T^*) = 1$, when the load completes a transit over the beam. Thus, below, T is assumed to satisfy $T \le T^*$.

The vertical acceleration of the mass particle is given by the Renaudot formula [10], which is the total time derivative of $w(\xi,t)$,

$$\frac{\mathrm{d}^2 w(\xi,t)}{\mathrm{d}t^2} = \left[w_{tt} + 2\dot{\xi}w_{xt} + \ddot{\xi}w_x + \dot{\xi}^2 w_{xx}\right]_{x=\xi(t)}. \tag{2.6}$$

The derivatives on the right-hand side are evaluated at the position of the mass $\xi(t)$. The horizontal acceleration is $\dot{v}(t) = \ddot{\xi} = f^*/m$.

Remark 2.2. We note here that there is an inaccuracy in formula (2.6) in [22], and the correct expression is (2.6). However, the mistake there did not affect the results since, all that was used was formula (2.7) there (when $v = const.$), which is exactly the same as (2.7) here.

When $v = \dot{\xi}$ is constant, then $\xi(t) = vt$, $\ddot{\xi} = 0$ and (2.6) reads

$$\frac{\mathrm{d}^2 w(vt,t)}{\mathrm{d}t^2} = \left[w_{tt} + 2vw_{xt} + v^2 w_{xx}\right]_{x=vt}. \tag{2.7}$$

Remark 2.3. In later stages of this work we plan to take into account friction into the horizontal motion of the mass. This may be done by using a beam-rod system. This, however, introduces considerable additional complexity which is not warranted at this stage.

The system is nonlinear and of unusual form and so it is natural to consider a weak or variational formulation, especially since the Dirac 'delta function', and its derivative, which are distributions, appear in (2.1), and so we expect the velocity w_t to be discontinuous at $x = \xi(t)$.

3. Existence

In this section we construct a variational formulation of the model, provide the assumptions on the input data, then state the existence result and provide its proof. First, we rewrite the system,

$$\begin{aligned}
&\rho w_{tt} + \frac{\mathrm{d}}{\mathrm{d}t}\left(m\delta(x-\xi)w_t(\xi,t)\right) + kw_{xxxx} + \gamma w_{txxxx} \\
&\qquad -(aw_x^2 - \overline{\nu}p)w_{xx} = \rho f + \delta(x-\xi)P, && (3.1)\\
&m\ddot{\xi} = f^*, && (3.2)\\
&w(0,t) = w_x(0,t) = 0, && (3.3)\\
&w(1,t) = w_x(1,t) = 0, && (3.4)\\
&w(x,0) = w_0(x), \quad w_t(x,0) = v_0(x). && (3.5)
\end{aligned}$$

Next, we derive a variational formulation for the model. Let V be the Hilbert space

$$V = \left\{u \in H^2(0,1) : u(0) = u_x(0) = u(1) = u_x(1) = 0\right\},$$

and let

$$H = L^2(0,1), \quad W = \text{closure of } V \text{ in } H^1(0,1).$$

These spaces contain the boundary conditions, since the beam is clamped at both ends. The problem is formulated in terms of mappings from $\mathcal{V}$ to its dual space $\mathcal{V}'$, where

$$\mathcal{V} \equiv \mathcal{L}^2(0,T;V), \quad \mathcal{W} \equiv L^2(0,T;W).$$

We begin with the inertial term and let $\psi(x) \in V$ and $\phi(t) \in C_c^\infty(0,T)$ and use $\psi(x)\phi(t)$ as a test function. We multiply the equation and integrate over space and time, thus,

$$\begin{aligned}
&\int_0^1 \int_0^T \frac{\mathrm{d}}{\mathrm{d}t}\left(m\delta(x-\xi)w_t(\xi,t)\right)\phi(t)\psi(x)\,\mathrm{d}t\mathrm{d}x \\
&= \int_0^1 \left(\left[\left(m\delta(x-\xi)w_t(\xi,t)\right)\phi(t)\psi(x)\right|_0^T\right. \\
&\quad \left. - \int_0^T \left(m\delta(x-\xi)w_t(\xi,t)\right)\phi'(t)\psi(x)\right]\mathrm{d}t\Big)\,\mathrm{d}x \\
&= -\int_0^T \int_0^1 \left(m\delta(x-\xi)w_t(\xi,t)\right)\phi'(t)\psi(x)\,\mathrm{d}x\mathrm{d}t \\
&= -\int_0^T m w_t(\xi,t)\,\phi'(t)\psi(\xi)\,\mathrm{d}t. \qquad (3.6)
\end{aligned}$$

Here, we used the boundary conditions and the fact that ϕ vanishes at $t = 0, T$. Next, we define the operator $B(t) : V \to V'$ as

$$\langle B(t)u, y\rangle = mu(\xi(t))\,y(\xi(t)).$$

It follows that $B(t)$ is symmetric and bounded because pointwise evaluation is continuous on V. Next, the usual arguments from calculus yield

$$\langle B'(t)u, y\rangle = \left(mu_x(\xi(t))\,y(\xi(t)) + mu(\xi(t))\,y_x(\xi(t))\right)\dot{\xi}(t). \qquad (3.7)$$

We assume that f^* is continuous and bounded, hence it follows from (3.2) that $\dot{\xi}$ is bounded and continuous. Therefore, continuity of pointwise evaluation on $H^1(0,L)$ guarantees that there exists a constant C, dependent on m and the bound for $\dot{\xi}$, such that

$$\langle B'(t)u, y\rangle \geq -C\left(\|u\|_V \|y\|_W + \|u\|_W \|y\|_V\right). \qquad (3.8)$$

Furthermore, we let $\varepsilon > 0$ be given, then we have the inequality

$$\|z\|_{H^1} \leq \varepsilon \|z\|_V + C_\varepsilon |z|_H$$

Applying it to (3.8) and adjusting the constants, we obtain,

$$\begin{aligned}
\langle B'(t)u, u\rangle &\geq -C\left(||u||_V\left(\varepsilon\|u\|_V + C_\varepsilon |u|_H\right)\right) \\
&\geq -\varepsilon ||u||_V^2 - C_\varepsilon |u|_H^2. \qquad (3.9)
\end{aligned}$$

While C_ε may be quite large ε can be made as small as desired. Also, (3.7) shows that B' is continuous as a map from V to V'.

For the sake of simplicity, we assume that the density $\rho = 1$, although the method below may be applied to a density that is inhomogeneous and possibly time dependent, $\rho = \rho(x,t)$. Using the boundary conditions, we find

$$\begin{aligned}
&\int_0^T \int_0^1 \left(kw_{xxxx} + \gamma w_{txxxx}\right)\psi(t)\,\phi(x)\,\mathrm{d}x\mathrm{d}t \\
&= \int_0^T \int_0^1 \left(kw_{xx} + \gamma w_{txx}\right)\psi(t)\,\phi_{xx}(x)\,\mathrm{d}x\mathrm{d}t.
\end{aligned}$$

Let $L : V \to V'$ be the operator

$$\langle Lu, w\rangle = \langle Lu, w\rangle_{V',V} \equiv \int_0^1 u_{xx} w_{xx}\mathrm{d}x.$$

Now, we consider the nonlinear term, and define $N : V \to V'$ by

$$\langle Nw, u\rangle \equiv -\int_0^1 (aw_x^2 - \overline{\nu}p)w_{xx}u\mathrm{d}x.$$

We also need an approximate operator which comes from truncating. To that end, let

$$Q_r(x) \equiv \begin{cases} x^2 \text{ if } |x| < r, \\ r^2 \text{ if } |x| \geq r. \end{cases}$$

Next, we consider the truncated operator

$$\langle N_r w, u\rangle \equiv -\int_0^1 (aQ_r(w_x) - \overline{\nu}p)w_{xx}u\mathrm{d}x.$$

Let $\Phi_r'(x) = Q_r(x)$, $\Phi_r(0) = 0$. Then, using the boundary conditions we obtain

$$\begin{aligned} \langle N_r w, w\rangle &= -\int_0^1 (aQ_r(w_x) - \overline{\nu}p)w_{xx}w\mathrm{d}x \\ &= -\int_0^1 (a\Phi_r'(w_x)w_{xx}w - \overline{\nu}pw_{xx}w)\,\mathrm{d}x \\ &= -\int_0^1 a\frac{d}{\mathrm{d}x}(\Phi_r(w_x))\,w\,\mathrm{d}x + \int_0^1 \overline{\nu}pw_{xx}w\mathrm{d}x \\ &= \int_0^1 a\Phi_r(w_x)\,w_x\,\mathrm{d}x + \int_0^1 \overline{\nu}pw_{xx}w\,\mathrm{d}x. \end{aligned}$$

Note that the first term is nonnegative. Below we derive an estimate for w in V that is independent of r and then by choosing r large enough we obtain a solution to the non-truncated problem. But first, we consider $\|N_r w - N_r\bar{w}\|_{V'}$.

$$\begin{aligned} |\langle N_r w - N_r\bar{w}, v\rangle| &\leq \left|\int_0^1 \overline{\nu}p(w_{xx} - \bar{w}_{xx})v\mathrm{d}x\right| + |a|\int_0^1 |\Phi_r(w_x) - \Phi_r(\bar{w}_x)|\,|v_x|\,\mathrm{d}x \\ &= \left|\int_0^1 \overline{\nu}p(w_x - \bar{w}_x)v_x\mathrm{d}x\right| + |a|\int_0^1 |\Phi_r(w_x) - \Phi_r(\bar{w}_x)|\,|v_x|\,\mathrm{d}x \\ &\leq \left|\int_0^1 \overline{\nu}p(w_x - \bar{w}_x)v_x\mathrm{d}x\right| + |a|\,K_r\int_0^1 |w_x - \bar{w}_x|\,|v_x|\,\mathrm{d}x \\ &\leq C_r\|w - \bar{w}\|_W\|v\|_W. \end{aligned}$$

Here, $K_r = 2r$ is the Lipschitz constant of Φ_r, and C_r is a positive constant that depends on r. Thus, since V is dense in W,

$$\|N_r w - N_r\bar{w}\|_{V'} \leq C_r\|w - \bar{w}\|_W. \tag{3.10}$$

To simplify slightly the presentation, we let $w(t) = w_0 + \int_0^t u(s)\,\mathrm{d}s$ and write the problem in terms of the beams velocity u.

We first consider the problem in which N is replaced with N_r. Our abstract formulation of the truncated problem becomes

$$((I + B(t))u)' + kLw + \gamma Lu + N_r w = f + \delta(\cdot - \xi)P, \tag{3.11}$$

$$w(t) = w_0 + \int_0^t u(s)\,\mathrm{d}s, \tag{3.12}$$

$$u(0) = v_0, \tag{3.13}$$

where

$$\langle\delta(\cdot - \xi)P, u\rangle \equiv \int_0^T P(t)\,u(t, \xi(t))\,\mathrm{d}t. \tag{3.14}$$

We now assume that $w \in C([0,T];V)$ is given. Then, it follows from the usual considerations (see, e.g., [21,23–25] and the many references therein) that there exists a solution u to (3.11)–(3.13) such that $u \in \mathcal{V}$, $u' \in \mathcal{V}'$. However, we do not know if (3.12) holds. It follows from (3.9) that

$$\gamma \langle Lu, u\rangle + \frac{1}{2}\int_0^T \langle (I+B')\, u, u\rangle \,\mathrm{d}t \geq \delta(\omega) \int_0^T \|u\|_V^2 \,\mathrm{d}s - C\,|u|_H^2,$$

which is sufficient to allow us to use the main result of [21] along with an exponential shift argument. Then, the monotonicity of L and the estimates for B' show that the solution u is unique. Next, assume that w and $\hat{w}$ are given and let (w,u) and $(\hat{w},\hat{u})$ be the corresponding solutions, hence,

$$\begin{aligned}((I+B(t))\,u)' + kLw + \gamma L(u) + N_r w &= f + \delta(\cdot - \xi)\,P,\\ ((I+B(t))\,\hat{u})' + kL\hat{w} + \gamma L(\hat{u}) + N_r \hat{w} &= f + \delta(\cdot - \xi)\,P.\end{aligned}$$

Then, we let

$$((I+B(t))\,(u-\hat{u}))' + kL(w-\hat{w}) + \gamma L(u-\hat{u}) + N_r w - N_r \hat{w} = 0$$

act on $u-\hat{u}$ and use the integration by parts theorems developed in [21] to obtain, for $\tilde{B}(t) \equiv I + B(t)$, the inequality

$$\begin{aligned}&\frac{1}{2}\left\langle \tilde{B}(u-\hat{u}), u-\hat{u}\right\rangle(t) + \frac{1}{2}\int_0^t \langle B'(u-\hat{u}), u-\hat{u}\rangle \,\mathrm{d}s\\ &+ k\,||w(t)-\hat{w}(t)||_V^2 + \gamma\int_0^t ||u-\hat{u}||_V^2 \,\mathrm{d}s \leq C_r\,||w(t)-\hat{w}(t)||_W^2.\end{aligned}$$

It follows from the compactness of the embedding of V into W that

$$\begin{aligned}&\frac{1}{2}|u-\hat{u}|_H^2(t) + \int_0^t \langle B'(u-\hat{u}), u-\hat{u}\rangle \,\mathrm{d}s + k\,||w(t)-\hat{w}(t)||_V^2 + \gamma\int_0^t ||u-\hat{u}||_V^2 \,\mathrm{d}s\\ &\leq \varepsilon\,\|w(t)-\hat{w}(t)\|_V^2 + C_{\varepsilon.r}\,|w(t)-\hat{w}(t)|_H^2.\end{aligned}$$

Now, we use the estimates in (3.9) for B' and obtain

$$\begin{aligned}&\frac{1}{2}|u-\hat{u}|_H^2(t) - \int_0^t \varepsilon\,\|u-\hat{u}\|_V^2 \,\mathrm{d}s - C_\varepsilon\int_0^t |u-\hat{u}|_H^2 \,\mathrm{d}s + k\,||w(t)-\hat{w}(t)||_V^2\\ &+\gamma\int_0^t ||u-\hat{u}||_V^2 \,\mathrm{d}s \leq \varepsilon\,\|w(t)-\hat{w}(t)\|_V^2 + C_{\varepsilon.r}\,|w(t)-\hat{w}(t)|_H^2,\end{aligned} \tag{3.15}$$

where ε can be chosen as small as desired.

We wish to use a fixed point argument. To that end for a given w let u be the solution of (3.11)–(3.13) that corresponds to w and we let

$$Fw(t) \equiv w_0 + \int_0^t u(s)\,\mathrm{d}s.$$

It follows from the estimates above that,

$$|Fw(t) - F\hat{w}(t)|_H \leq \int_0^t |u(s)-\hat{u}(s)|\,\mathrm{d}s.$$

Choosing ε sufficiently small in (3.15), we find that there is a constant $C_{k,\gamma,r} > 0$, depending on k, r, γ such that

$$|u-\hat{u}|_H(t) \leq C_{k,\gamma,r}\,|w-\hat{w}|_H(t),$$

and so, there is another constant C that depends on k, γ, r such that

$$|Fw(t) - F\hat{w}(t)|_H \leq C\int_0^t |w-\hat{w}|_H(s)\,\mathrm{d}s.$$

It follows from iteration of the inequality that a high enough power of F is a contraction map on $C([0,T];H)$ and so there exists a unique fixed point w of F, hence

$$w(t) = Fw(t) = w_0 + \int_0^t u(s)\,\mathrm{d}s,$$

which is the unique solution of (3.11)–(3.13). This has proved the following theorem.

Theorem 3.1. *For each $r > 0$ there exists a unique solution w to the approximate problem (3.11)–(3.13) and it satisfies $w \in \mathcal{V}$ and $((I + B(\cdot))w)' \in \mathcal{V}'$.*

Actually, when r is sufficiently large, this estimate shows the existence of a unique solution for the original problem without the truncation. To see this, it suffices to obtain an estimate on w_x that is independent of r. To that end, we let (3.11) act on u. Then, using the estimate for B' in (3.9), we obtain

$$\begin{aligned}\frac{1}{2}|u(t)|_H^2 - \varepsilon\int_0^t ||u(s)||_V^2\,\mathrm{d}s - C_\varepsilon\int_0^t |u(s)|_H^2\,\mathrm{d}s + k||w(t)||_V^2 - k||w_0||^2 + \gamma\int_0^t ||u||_V^2\,\mathrm{d}s \\ - \int_0^t\int_0^1 (aQ_r(w_x) - \overline{\nu}p)w_{xx}u\,\mathrm{d}x\mathrm{d}s \leq C_\varepsilon + \varepsilon\int_0^t ||u(s)||_V^2\,\mathrm{d}s,\end{aligned} \tag{3.16}$$

where C_ε depends on f and P. We now consider the nonlinear term and using the boundary conditions, we find

$$\begin{aligned}-\int_0^t\int_0^1 (aQ_r(w_x) - \overline{\nu}p)w_{xx}u\mathrm{d}x\mathrm{d}s &= -\int_0^t\int_0^1 a\Phi_r(w_x)_x\,u\mathrm{d}x\mathrm{d}s + \int_0^t\int_0^1 \overline{\nu}pw_{xx}u\mathrm{d}x\mathrm{d}s \\ &\geq \int_0^t\int_0^1 a\Phi_r(w_x)\,u_x\mathrm{d}x\mathrm{d}s - C\left(\int_0^t ||w||_V^2\,\mathrm{d}s + \int_0^t |u|_H^2\,\mathrm{d}s\right).\end{aligned}$$

Letting $\Psi_r(x) = \int_0^x \Phi_r(y)\,dy$, it follows that $\Psi_r(x) \geq 0$ and then,

$$\begin{aligned}&= \int_0^1 a\Psi_r(w_x)\,\mathrm{d}x - \int_0^1 a\Psi_r(w_{0x})\,\mathrm{d}x - \left(\int_0^t \varepsilon||w||_V^2\,\mathrm{d}s + C_\varepsilon\int_0^t |u|_H^2\,\mathrm{d}s\right) \\ &\geq -\int_0^1 a\Psi_r(w_{0x})\,\mathrm{d}x - \left(\int_0^t \varepsilon||w||_V^2\,\mathrm{d}s + C_\varepsilon\int_0^t |u|_H^2\,\mathrm{d}s\right) \\ &\geq -C - C\left(\int_0^t ||w||_V^2\,\mathrm{d}s + \int_0^t |u|_H^2\,\mathrm{d}s\right),\end{aligned}$$

for a constant C that is independent of r, for all r sufficiently large. Here, we used the fact that w_{0x} is bounded since $w_0 \in V$. Thus, (3.16) implies

$$\begin{aligned}\frac{1}{2}|u(t)|_H^2 - \varepsilon\int_0^t ||u(s)||_V^2\,\mathrm{d}s - C_\varepsilon\int_0^t |u(s)|_H^2\,\mathrm{d}s + k||w(t)||_V^2 - k||w_0||_V^2 + \gamma\int_0^t ||u||_V^2\,\mathrm{d}s \\ - \left(C + C\left(\int_0^t ||w||_V^2\,\mathrm{d}s + \int_0^t |u|_H^2\,\mathrm{d}s\right)\right) \leq C_\varepsilon + \varepsilon\int_0^t ||u(s)||_V^2\,\mathrm{d}s.\end{aligned}$$

Choosing ε small enough, depending on γ, we obtain

$$|u(t)|_H^2 + \frac{\gamma}{2}\int_0^t ||u||_V^2\,\mathrm{d}s + k||w(t)||_V^2 \leq C_\varepsilon + k||w_0||_V^2 + C\int_0^t ||w||^2\,\mathrm{d}s + \int_0^t |u|_H^2\,\mathrm{d}s.$$

Then, Gronwall's inequality establishes a bound for $||w(t)||_V$ that is independent of r. This yields the following corollary, which is the main theoretical result in this work.

Theorem 3.2. *There exists a unique solution u to the problem*

$$((I + B(t))u)' + kLw + \gamma Lu + Nw = f + \delta(\cdot - \xi)P, \tag{3.17}$$

$$w(t) = w_0 + \int_0^t u(s)\,\mathrm{d}s, \tag{3.18}$$

$$u(0) = v_0, \tag{3.19}$$

$u \in \mathcal{V}$ and $((I + B(\cdot))u)' \in \mathcal{V}'$. Moreover, when r is chosen large enough this is the unique weak solution of the original problem, (3.1)–(3.5), without the truncation.

We conclude that there exists a unique weak solution of the model. We note that although $\gamma > 0$, it may be as small as we wish, however, the limit $\gamma \to 0$ cannot be obtained from these considerations.

4. Numerical algorithm

We develop a numerical scheme for the model, and the results of its implementation are presented in the following section.

There are numerous methods to obtain numerical approximations for initial–boundary problems. In some problems, and ours is of such a type, the standard methods either fail or cannot be directly applied to the differential equations. In this problem the governing equation is nonlinear and has varying coefficients. In the classical finite element method, FEM, such problems are simplified and the nonlinear terms are linearized, which may cause the results to diverge from the exact ones. In our model, this occurs when the inertial point crosses the element's boundary or passes to a successive time layer in the process of time integration of the equation of motion. Such a traveling point carries the momentum perpendicular to the beam's axis, along the beam. In such a case, the numerical algorithms based on routine approach of FEM do not provide correct results.

To address this problem, we used the space–time finite element approach. Continuous approximations were applied to both the spatial and temporal variables at the same time [26–28]. This allows for a weak formulation of the problem that cannot be simply formulated while separating time from space. There exist broad literature devoted to space–time finite element method, STFEM, for various problems, see, e.g., [29–31] and the references therein.

The main difference between the classical FEM and the STFEM lies in the interpolation functions:

$$\mathbf{q}(x,t) = \mathbf{N}(x) \cdot \mathbf{T}(t)\,\mathbf{q}_e \quad \text{(FEM)}, \qquad \mathbf{q}(x,t) = \mathbf{N}(x,t)\,\mathbf{q}_e \quad \text{(STFEM)}.$$

In FEM the interpolation in space $\mathbf{N}(x)$ and time $\mathbf{T}(t)$ are done separately while in STFEM the interpolation is carried on jointly $\mathbf{N}(x,t)$. Thus, FEM can be considered as a particular case of STFEM.

We discretize the equation of motion (2.1) using space–time rectangular finite elements, depicted in Fig. 3, where the element subdomain is

$$\Omega_{bh} = \{(x,t) : 0 \le x \le b,\ 0 \le t \le h\}.$$

Here, $h = \triangle t$ is the time step, so that if T is the final time, we have $n_T = T/h$ time steps and $n_S = 1/b$ spacial elements (recall that $L = 1$).

We take into account the pure bending process described by the 4th order x-derivative (see, (2.1)). In this beam model, the influence of the shear forces on the potential energy, and therefore on the deflection, are neglected. Then, the angle of rotation of the cross section is directly joined with the deflected neutral axis of the beam. We use both deflections and rotations at nodal points of each element. Thus, there are

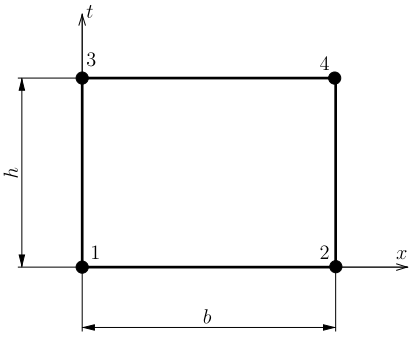

Fig. 3. A space–time finite element domain Ω_{bh}.

four degrees of freedom at each time layer of the element that allow to determine a third order polynomial in space. We use a velocity variant of the space–time discretization, therefore, the velocity in the beam finite element is represented by the nodal velocity parameters in two successive time steps. We denote the current state, which just has been obtained, by $\mathbf{v}^t$ and the unknown state at the next time step by $\mathbf{v}^{t+h}$. Thus, we have

$$\mathsf{v}(x,t) = \left(1 - \frac{t}{h}\right)\mathbf{N}\mathbf{v}^t + \frac{t}{h}\mathbf{N}\mathbf{v}^{t+h}, \tag{4.1}$$

where

$$\begin{bmatrix}\mathbf{v}^t \\ \mathbf{v}^{t+h}\end{bmatrix} = \begin{bmatrix}\mathsf{v}_1 & \dot{\psi}_1 & \mathsf{v}_2 & \dot{\psi}_2 & \mathsf{v}_3 & \dot{\psi}_3 & \mathsf{v}_4 & \dot{\psi}_4\end{bmatrix}^{\mathsf{T}}, \tag{4.2}$$

is the nodal velocity vector and the shape functions $\mathbf{N}$ are given by

$$\mathbf{N} = [N_1, N_2, N_3, N_4], \tag{4.3}$$

are chosen as

$$N_1 = 1 - 3\frac{x^2}{b^2} + 2\frac{x^3}{b^3}, \qquad N_2 = x - 2\frac{x^2}{b} + \frac{x^3}{b^2},$$
$$N_3 = 3\frac{x^2}{b^2} - 2\frac{x^3}{b^3}, \qquad N_4 = -\frac{x^2}{b} + \frac{x^3}{b^2}.$$

We see that the velocity vector v in (4.1) is interpolated from eight nodal values: four that are known from a previous time t and four unknown at time $t + h$. Now, we use (4.1) to calculate the displacements in the element,

$$\begin{aligned}\mathsf{w}(x,t) &= \mathsf{w}_0(x) + \int_0^t \mathsf{v}(x,t)\mathrm{d}t \\ &= \mathbf{N}\mathbf{w}^t + \left(t - \frac{t^2}{2h}\right)\mathbf{N}\mathbf{v}^t + \frac{t^2}{2h}\mathbf{N}\mathbf{v}^{t+h},\end{aligned} \tag{4.4}$$

where the nodal displacement vector $\mathbf{w}^t$ is known and composed of the deflections w and rotations ψ given at two nodes of the space–time element at time t. The differential equation (2.1) allows us to write the virtual work in the finite element as follows

$$\begin{aligned}\Pi = \int_\Omega \mathsf{v}^* \big\{&\rho\mathsf{w}_{tt} + k\mathsf{w}_{xxxx} - a\mathsf{w}_x^2\mathsf{w}_{xx} + \overline{\nu}p\mathsf{w}_{xx} \\ &+ \delta(x - vt)m\mathsf{w}_{tt}(vt,t) - \delta(x - vt)P\big\}\,\mathrm{d}x\mathrm{d}t,\end{aligned} \tag{4.5}$$

where the virtual velocity v^* with the parameter α is given by

$$\mathsf{v}^*(x,t) = \delta(t - \alpha h)\left(\mathbf{N}\mathbf{v}^*\right)^{\mathsf{T}}.$$

We use this form, chosen from the various possible functions of virtual velocity distributions, because of the simplicity of the time integration of the energy functional Π and simple stability control. Here, $\alpha \in [0,1]$ is a parameter that defines the equilibrium point in the time layer (similarly to β in the Newmark time integration scheme). It affects the accuracy and stability of the resulting time integrating scheme (for details see [32]). Integrating, formally, by parts the virtual work expression (4.5) leads to the following expression

$$\begin{aligned}\Pi =& k\int_\Omega \mathsf{v}^*_{xx}\mathsf{w}_{xx}\,\mathrm{d}x\,\mathrm{d}t + \int_\Omega \mathsf{v}^*\left\{\rho\mathsf{v}_t - a\mathsf{w}_x^2\mathsf{w}_{xx} + \overline{\nu}p\mathsf{w}_{xx}\right.\\ &+ \left.\delta(x-vt)m(\mathsf{v}_t + 2v\mathsf{v}_x + v^2\mathsf{w}_{xx})\big|_{x=vt} - \delta(x-vt)P\right\}\mathrm{d}x\,\mathrm{d}t. \end{aligned} \tag{4.6}$$

To proceed with the numerical scheme, we need the following matrices: the element mass and stiffness characteristic matrices are given by

$$\mathbf{M} = \rho\begin{bmatrix} \frac{13b}{35} & \frac{11b^2}{210} & \frac{9b}{70} & \frac{-13b}{420} \\ \frac{11b^2}{210} & \frac{b^3}{105} & \frac{13b^2}{420} & \frac{-b^3}{140} \\ \frac{9b}{70} & \frac{13b^2}{420} & \frac{13b}{35} & \frac{-11b^2}{210} \\ \frac{-13b^2}{420} & \frac{-b^3}{140} & \frac{-11b^2}{210} & \frac{b^3}{105} \end{bmatrix},$$

and

$$\mathbf{K} = k\begin{bmatrix} \frac{12}{b^3} & \frac{6}{b^2} & \frac{-12}{b^3} & \frac{6}{b^2} \\ \frac{6}{b^2} & \frac{4}{b} & \frac{-6}{b^2} & \frac{2}{b} \\ \frac{-12}{b^3} & \frac{-6}{b^2} & \frac{12}{b^3} & \frac{-6}{b^2} \\ \frac{6}{b^2} & \frac{2}{b} & \frac{-6}{b^2} & \frac{4}{b} \end{bmatrix} + \overline{\nu}p\begin{bmatrix} \frac{6}{5b} & \frac{11}{10} & \frac{-6}{5b} & \frac{1}{10} \\ \frac{1}{10} & \frac{2b}{15} & \frac{-1}{10} & \frac{-b}{30} \\ \frac{-6}{5b} & \frac{-1}{10} & \frac{6}{5b} & \frac{-11}{10} \\ \frac{1}{10} & \frac{-b}{30} & \frac{-1}{10} & \frac{2b}{15} \end{bmatrix}.$$

To deal with the nonlinearity, we use a term in which the nonlinearity is frozen at the time t so that $\mathbf{w}^t$ and $\mathbf{v}^t$ are known,

$$\mathbf{K}_n = a\int_0^b \mathbf{N}^{\mathsf{T}}\left[\mathbf{N}_x\mathbf{w}^t + (\alpha - 0.5\alpha^2)h\mathbf{N}_x\mathbf{v}^t + 0.5\alpha^2 h\mathbf{N}_x\mathbf{v}^{t+h}\right]^2\mathbf{N}_{xx}\,\mathrm{d}x. \tag{4.7}$$

The explicit matrix form of $\mathbf{K}_n$ is provided in the Appendix.

The general matrices representing the moving mass were derived by using linear shape functions as described in [33],

$$\mathbf{M}_m = m\begin{bmatrix} (1-\kappa)^2 & 0 & \kappa(1-\kappa) & 0 \\ 0 & 0 & 0 & 0 \\ \kappa(1-\kappa) & 0 & \kappa^2 & 0 \\ 0 & 0 & 0 & 0 \end{bmatrix},$$

$$\mathbf{C}_m = \frac{2mv}{b}\begin{bmatrix} \kappa-1 & 0 & 1-\kappa & 0 \\ 0 & 0 & 0 & 0 \\ -\kappa & 0 & \kappa & 0 \\ 0 & 0 & 0 & 0 \end{bmatrix},$$

$$\mathbf{e}^t_m = \frac{mv}{bh}\begin{bmatrix} (1-\kappa)(\mathsf{w}_2^{i+1} - \mathsf{w}_2^i - \mathsf{w}_1^{i+1} + \mathsf{w}_1^i) \\ 0 \\ \kappa(\mathsf{w}_2^{i+1} - \mathsf{w}_2^i - \mathsf{w}_1^{i+1} + \mathsf{w}_1^i) \\ 0 \end{bmatrix}.$$

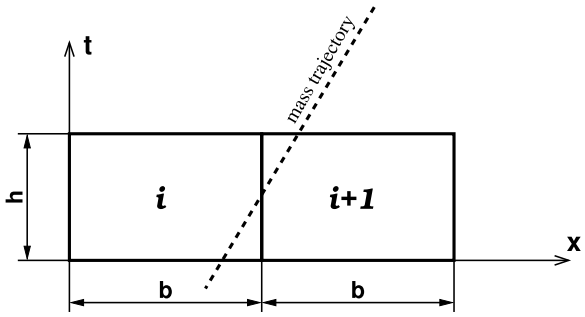

Fig. 4. The transition of the mass between two elements.

The upper indices i and $i+1$ are the numbers of neighboring spatial elements traversed by the inertial particle (Fig. 4). The lower indices 1 and 2 correspond to left and right nodes in each neighboring element.

The moving force vector is given as

$$\mathbf{F}^t = P \begin{bmatrix} 1-\kappa \\ 0 \\ \kappa \\ 0 \end{bmatrix},$$

where $\kappa \in [0,1]$ is parameter that describes current position of the moving load in finite element. Finally, the minimization of the functional in (4.6) and the above matrices lead to our numerical scheme, which is of the marching in time type.

Algorithm 4.1. Given $\mathbf{w}^t$ and $\mathbf{v}^t$, as well as $\mathbf{e}_m^t$ and $\mathbf{F}^t$, find $\mathbf{w}^{t+h}$ and $\mathbf{v}^{t+h}$ by solving the system

$$\begin{aligned} &\left[\mathbf{M}/h + \mathbf{M}_m/h + \alpha\mathbf{C}_m + 0.5\alpha^2 h(\mathbf{K}-\mathbf{K}_n)\right]\mathbf{v}^{t+h} \\ &- \ \left[\mathbf{M}/h + \mathbf{M}_m/h - (1-\alpha)\mathbf{C}_m \right. \\ &\left. -(\alpha - 0.5\alpha^2)h(\mathbf{K}-\mathbf{K}_n)\right]\mathbf{v}^t \\ &+ \ (\mathbf{K}-\mathbf{K}_n)\mathbf{w}^t + \mathbf{e}_m^t - \mathbf{F}^t = 0\,, \end{aligned} \tag{4.8}$$

and

$$\mathbf{w}^{t+h} = \mathbf{w}^t + h[(1-\alpha)\mathbf{v}^t + \alpha\mathbf{v}^{t+h}]\,. \tag{4.9}$$

The system is a linearized version of the nonlinear original system.

5. Numerical simulations

The algorithm of Section 4 was implemented and run on a PC and we present here six numerical simulations of the model done by realizing this algorithm. These depict: (i) comparison of the dynamics of the Gao and the linear Euler–Bernoulli beams; (ii) comparison between the massless applied force and the load applied to a mass; (iii) a study of the dependence of the dynamics on the traction p; (iv) the system behavior for different compressive tractions; (v) different velocities; and (vi) multiple passes of the mass over the span of the rail.

For the sake of simplicity, we assumed that there were no additional external distributed forces, $f = 0$; the beam was elastic, $\gamma = 0$; the term with δ' was neglected; and the ends were simply supported. We studied moderately large displacements of a moderately thick Gao beam (Figs. 1, 2) of length L (scaled to be 1) that was affected by a moving point load P that was applied to a mass m our directly to the be a, the massless case, that were traveling at constant speed v. It may be of interest to relax some of these assumptions,

especially that $v = const.$ The assumption that $v = const.$ makes Eq. (2.2) unnecessary. We note that while in [22] the traction at $x = 1$ was assumed to vanish and so there was no possibility for the beam to buckle, here we let $p > 0$ (compressive) and so the system may buckle when $p > p^*$, where p^* is the critical value (see, e.g., [5–7]). We return to this point below and study this in more details.

The time integration of the algorithm for the data listed below was 10 μs. The beam was divided into 100 finite elements with 202 degrees of freedom. The nonlinear terms were computed iteratively, hence each time step took relatively longer time. The time it took for each simulation was about 48 s during 20,000 time steps for $\alpha_v = 0.3$ and $p = 0.01$, which was the time it took the load to travel the entire span. Most of computing time was spent on recalculating the matrices related to the nonlinear effects. It was noticed, however, that by increasing the time step and allowing for a larger error, the task could be performed in 10–20 s on a single processor core. As was noted in [22, Section 4], to avoid the appearance numerical oscillations because of the nonlinear terms in the equations, we used an analytical evaluation of the coefficients, eliminating this problem.

The data set for a steel beam used in the simulations was:
$L = 100$ [cm],
$\beta = 0.015$,
$\tilde{\nu} = 0.3$, $\rho = 7.7\frac{\beta^2 L^2}{\pi} = 5.5175$ [g/cm]
$k = 0.57\frac{\beta^4 L^4}{4\pi^3} = 0.0233$ [g cm^3/μs^2],
$a = 3.105\frac{\beta^2 L^2}{\pi} = 2.2249$ [g cm/μs^2],
$v = \frac{\pi\sqrt{k/\rho}}{L}\alpha_v = 0.002\,\alpha_v$ [cm/μs],
$m = 100\rho L = 55175$ [g]
$P = mg = 5.4071 * 10^{-5}$ [g cm/μs^2],
$p^* = 0.71$ [g cm/μs^2],
$g = 9.8{\cdot}10^{-10}$ [cm/μs^2].

We used a nonstandard unit system [cm, g, μs] that allowed us to have all the values in the same range, which improved the conditioning of the system of algebraic equations and reduced the truncation errors.

We turn to describe the simulation results, which provide considerable insight into the system's dynamics. The first set of computer experiments compares the vibrations of the Gao beam with those of the linear Euler–Bernoulli beam, when $p = 0$, so that the comparison is valid. The simulations exhibit the basic difference in the dynamics of the two beam models and, as expected, the Gao beam behaves well for larger oscillations while the linear beam's oscillations become unphysical, implying that the Euler–Bernoulli beam may be used only with small loads and small amplitudes. The comparison between the two beams, when the load is massless is depicted in Fig. 5, and when the load acts on a mass, in Fig. 6.

In the massless case, although the trajectories' shapes have similar forms, the scales and the amplitudes of the vibrations are very different. Indeed, the amplitudes of the Euler–Bernoulli beam are very large and exceed any reasonable use of a linearized system. Thus, as was noted above, the linear model can be useful only when the loads are small. The Gao beam, on the other hand, behaves much better and the amplitudes are very reasonable. It exhibited stiffening with the amplitude and in the example the amplitudes were ten-fold smaller. We note that multiple passages of the point force without inertia have similar trajectories, both at successive periods and in both beam models, but not equal in value. However, the lack of a mass leads to spurious oscillations created by the numerics that can clearly be seen. This comparison is very instructive concerning the applicability of the two models.

Different responses were exhibited in the case of the inertial load ($m > 0$), Fig. 6, were the differences between the two models were even more pronounced. Whereas the Gao beam exhibited smooth regular oscillations, the Euler–Bernoulli beam oscillated wildly with unreasonable form and amplitude. The advantage of using the Gao beam to obtain meaningful simulations was evident. Moreover, we notice that the inertia of the mass leads to the smoothing of the oscillations with good accuracy and no visible spurious oscillations. As

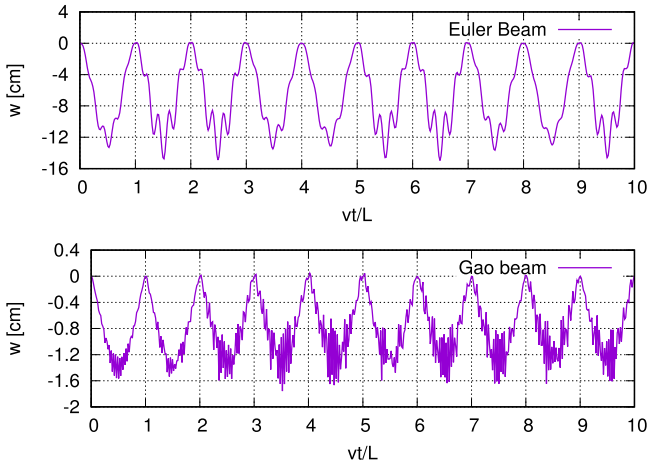

Fig. 5. Comparison of the load trajectory and the vibrations of a linear Euler–Bernoulli and the Gao beam models, for $m = 0$ and $p = 0$. Notice the different vertical scales.

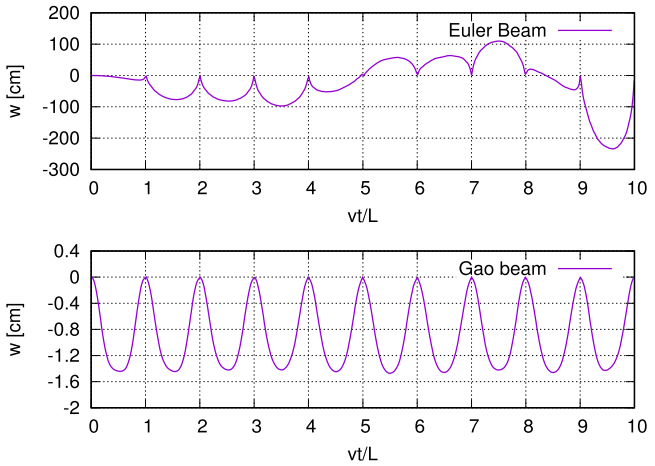

Fig. 6. Comparison of the load trajectory and the vibrations between a linear Euler–Bernoulli beam model and the Gao one, for $m > 0$ and $p = 0$. Notice the different scales.

we discuss below, multiple passages of the point force without inertia produced similar shapes of trajectories at successive periods and in both beam models.

To gain deeper insight into the system dynamics, we compared the behavior of the Gao model when the load acted on a mass m (the inertial case), or acted directly on the beam, (the massless or non-inertial case), for six different values of the horizontal compressive traction p. In all the cases, we chose the values of the compressive horizontal traction p to be above the critical value p^* so that the beam exhibited buckling.

Numerical estimate of p^*, depicted in Fig. 7, showed it to be about $p^* = 0.71$. Below this value the beam vibrated about the zero equilibrium point, while above it about a buckled state. A study of the vibrations of the mid-point of the Gao beam, without the moving load, near the critical value p^* in the cases $p = 0.600, 0.708, 0.710$ and 0.750 is depicted in Fig. 8. We note that there is no effective analytic way to determine p^*.

The six numerical experiments are depicted in Fig. 9. It is clearly seen that the frequency of the oscillations increases with p. The difference between the inertial and massless cases was substantial and the heavy mass changed the frequency considerably, although the amplitudes remained comparable. The importance

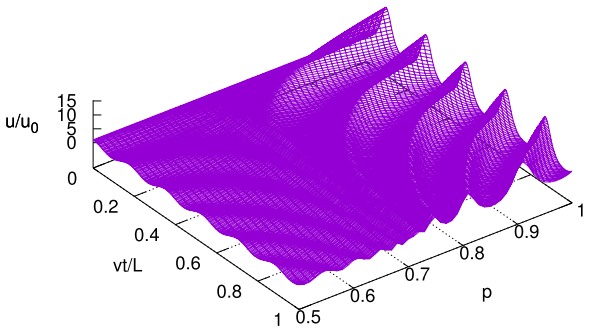

Fig. 7. The relative amplitude of the midpoint of the beam related to the amplitude of the initial deflection u_0 for various values of p. The value $p^* = 0.71$ divides the buckled from the non-buckled states.

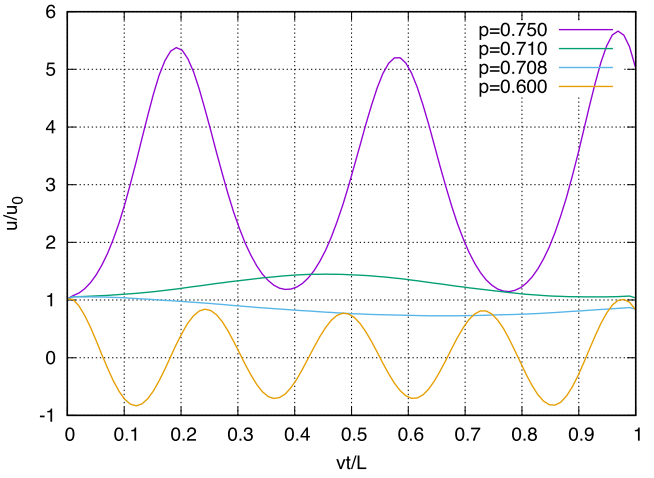

Fig. 8. The system oscillations at four values of p near the critical value $p^* = 0.71$. The vibrations with $p = 0.750$ are about a buckled state.

of adding the mass in railway applications was mentioned in the introduction, and these results show its importance. We also note that the contact point of P or the mass, was above the neutral axis (i.e., $w = 0$), in the cases of $p = 4.5$ and $p = 6.0$, while for p was below $p = 4.5$ or $p = 7.5$ the contact point was below $w = 0$. The behavior is well visible in Fig. 10, which depicts the deformed axes of the beam in time.

The fifth set of simulations investigated the system's response to three different load velocities. It was found, Fig. 11, that a slow motion of the load, $\alpha = 0.005$, generated a high number of oscillations during the load's transit. When the speed was increased ten-fold, to $\alpha = 0.05$, the transit time was reduced accordingly and so was the number of oscillations. The load trajectory in the quasi-static case was computed with $\alpha = 0$, and the vertical oscillations were related to the static deflection of the Gao span when the load P had been placed at mid-point. It was found that the trajectory of the point differed significantly from the classical sinusoidal trace. The system, because of the nonlinear term, exhibited higher stiffness in the deflected state while it was softer near the zero deflection, and the quasistatic line that corresponds to the equilibrium state was shifted towards deflection maxima.

In the sixth set, we investigated the system response to multiple loading of the span with a single inertial point load traveling in sequence over the beam. As can be seen in Fig. 12, a completely different response was exhibited for the inertial load, and resulted in unexpected scenarios of displacements. The point mass that entered the beam for the second time moved on a deformed beam that was vibrating because of the previous passage. Depending on the transit state, the load entering the beam either added energy or removed

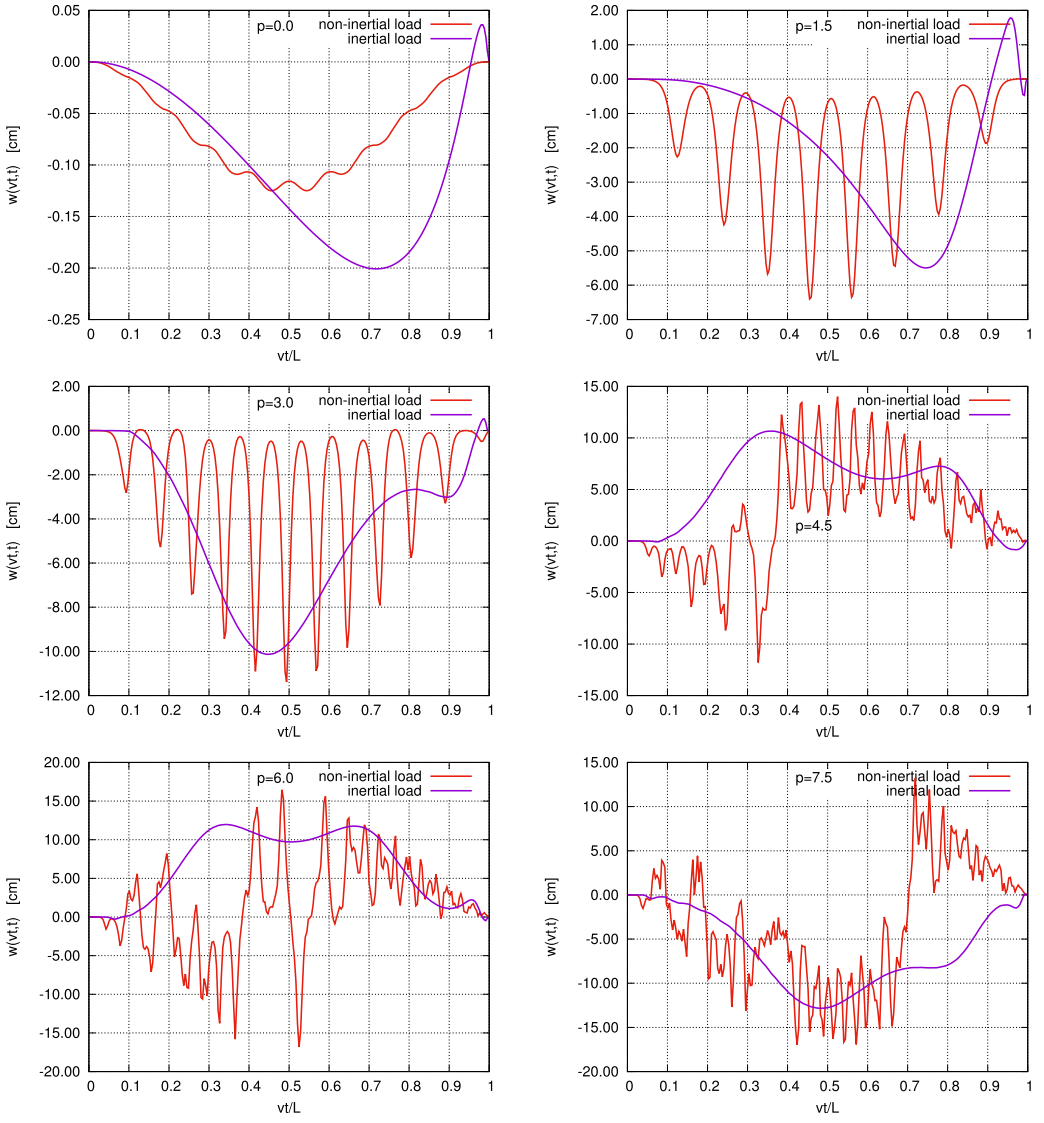

Fig. 9. Comparison between the system vibrations with inertial ($m > 0$) and non-inertial ($m = 0$) loads for six values of the horizontal compressive traction p, where $p > p^*$, and the beam is buckled. The inertia reduces the frequency of the oscillations, which seem to be much more regular.

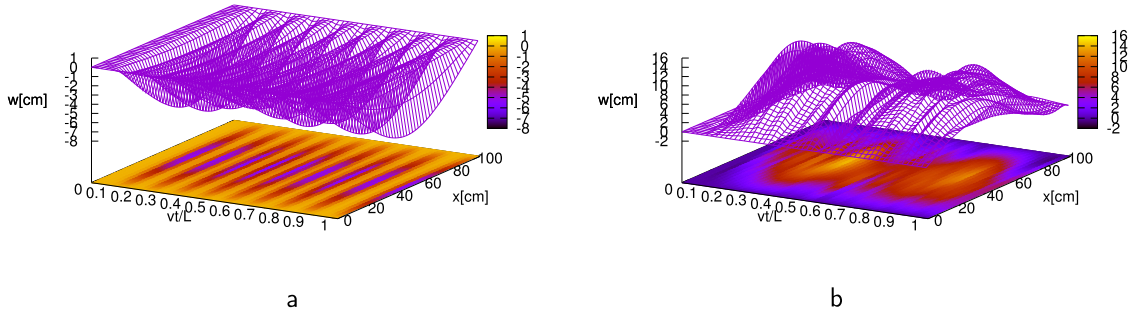

Fig. 10. Displacements in time for $\alpha_v = 0.05$, $\beta = 0.15$ for: (a) massless load with $p = 1.5$ and (b) inertial load with $p = 4.5$.

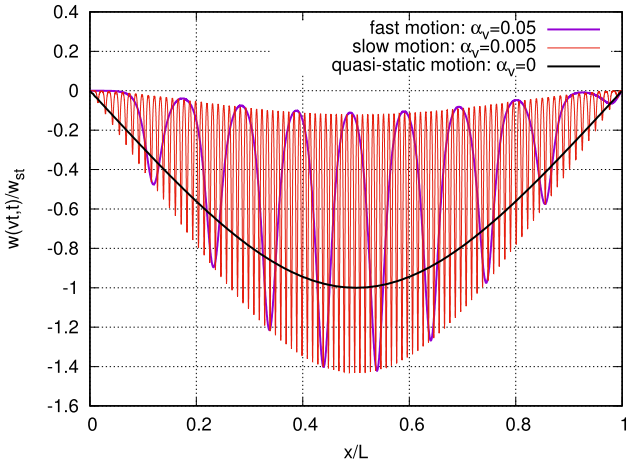

Fig. 11. Comparison of load trajectory at various speeds with $m = 0$ and $p = 1.5$, $\beta = 0.15$.

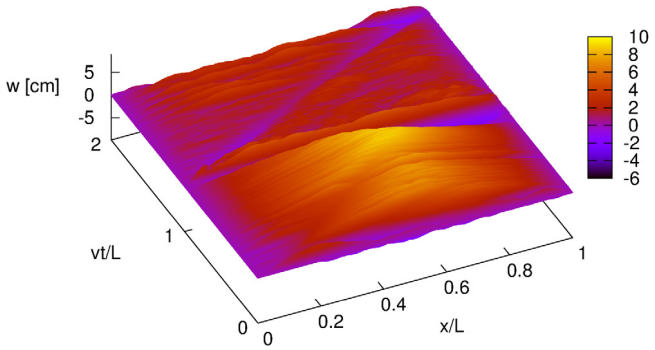

Fig. 12. The displacement $w(t)$ during two consecutive passages of the mass, $p = 85$.

it. Indeed, the system with the inertial moving load was non-conservative and the mass started its motion with zero vertical velocity and exited with non-zero vertical velocity. That is also why the moving inertia stabilized the motion. In the case of a faster motion of the mass on the support, high gradients of trajectories, i.e., the contact points of the beam with the load, were observed both in the analysis [34,35] and numerical simulations. High gradients of the beam axis appeared and the non-linear terms in the model led to large values. That is why at high speeds the system's response was more sensitive to the various parameters. Furthermore, one can observe positive displacements of some segments of the beam even though the vertical force vector pointed downward. The first passage raised the beam axis and during the second passage the smoothing influence of the moving mass was visible. This was depicted in Fig. 13, too.

For the sake of completeness, we also investigated the system behavior in the inertial case as p was increased within the three ranges $[0, 1]$, $[0, 10]$ and $[0, 100]$. We found that there was a progressive shift from the importance of the nonlinear Gao term to the linear term with p, and this shifted the type of the vibrations from those of a bending beam to those of a string. The progressive changes in the vibrations as the beam became softer can be clearly seen in the three parts of Fig. 13. Note the different vertical scales in the figure. First, when the values of p were small, in the range $[0, 1]$, the structure vibrated in the bending range with a relatively low contribution of the string vibrations. Indeed, at the low range of p, the bending was the main phenomenon. We expected gradual change of the vibrations during the first passage and more significant changes in successive passages of the mass. Fig. 13a depicts the curves for p up to 1.0, while Fig. 13b and c exhibit values of p in the ranges $[0, 10]$ and $[0, 100]$, respectively. In the higher range the wave

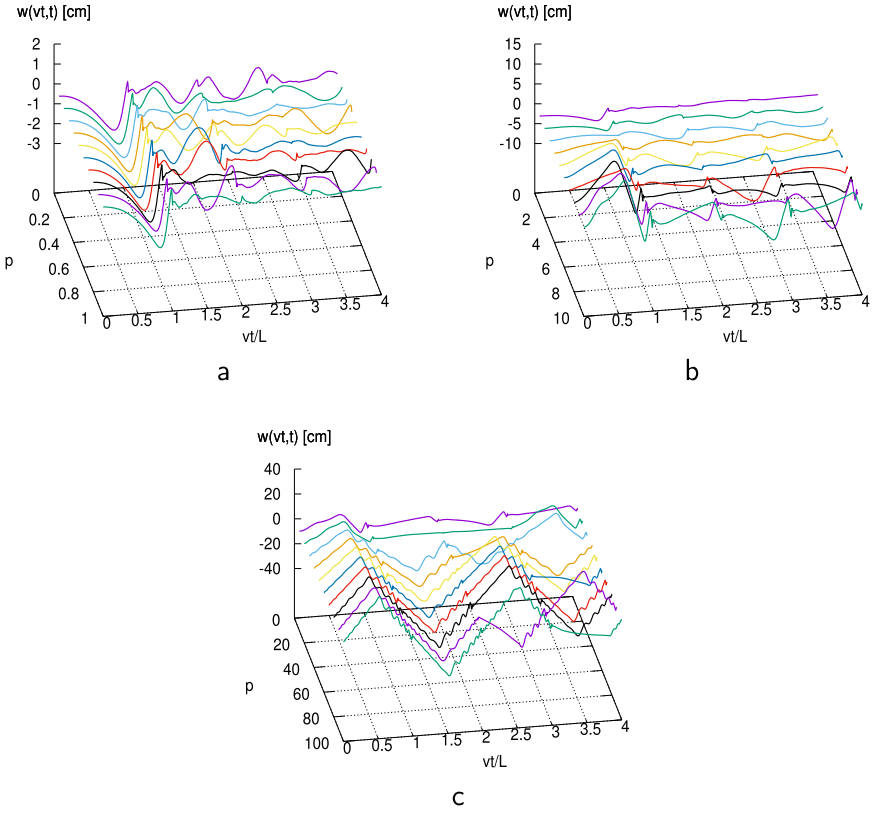

Fig. 13. Load trajectories for three ranges of p. The range $[0, 1]$ is top-left, $[0, 10]$ is top-right, $[0, 100]$ is bottom.

phenomenon that was dominant was of the string or axially loaded bar. At moderate p (Fig. 13 top-right) the process starts to elevate the follower point. This fact is visualized better in Fig. 12. The second passage led to flatter surface in the figure.

To see this transition from a bending beam mode to a string mode, we performed a numerical experiment with $p = 100$, and $\Delta t = 0.1$. Fig. 14 depicts the displacements in time of the moving mass. The high value of the traction p makes the bending stiffness practically negligible and the displacements caused by the load become large and non-physical. Moreover, we observed two waves: one that had a longer wave-length and was caused by reflections of the waves from the supports, while the second one had high frequency. In the initial stage (up to $vt/L = 0.1$) the solution was unstable and switched between two trajectories: downwards and upwards. Then, the motion of the loaded follower point took place along the straight segments that depended on the load velocity, however, not in the way known from the theory of waves in a string. Generally, the numerical solution in this case was sensitive to all of the problem parameters, together with the time step of numerical integration.

The increased axial force p resulted in another feature of the solution. The early stage of the motion of the traveling load influenced the character of the subsequent vibrations. The subjected part of the beam bent down in the direction of the load, but then the remote part of the beam was lifted up due to the rotation around the center of the inertia of the neighboring part of the beam. The axial compression intensified and consolidated this process.

Finally, we note that:

- The vibrations during the first passage that started with zero initial vertical velocity was similar for the various velocities and compressive tractions p.

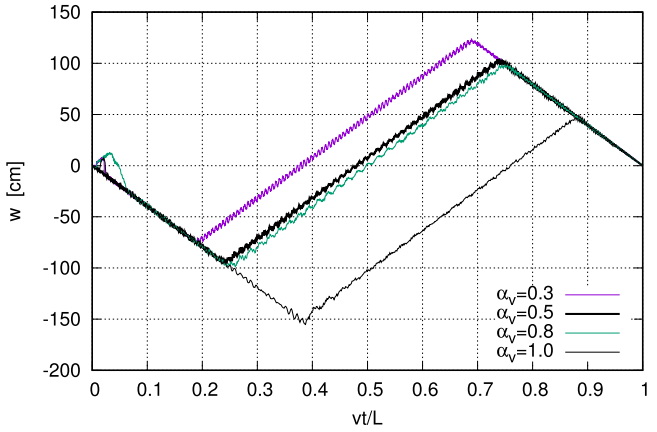

Fig. 14. String-like vibration in the case of a high axial compression $p = 100$ for four different speeds.

- Computationally, increasing p required a decrease in the time step. The same was found when the spatial mesh was refined.
- In order to not to dominate the bending effect, p should be small to moderate. When p was relatively large, the Gao beam started to vibrate as a highly tensioned string and hyperbolic wave effects were observed.

6. Conclusions and comments

This work studies the motion of a load that may be massless or with mass, on a rail modeled by the Gao nonlinear beam. It extends the research in [22] to the case of dynamic vibrations when the traction p at $x = L(= 1)$ is positive and sufficiently large to cause buckling. The differences between the results here and those in [22] are substantial, indicating that this line of research is worth pursuing further.

The model, (2.1)–(2.6), is in the form of a nonlinear dynamic equation for the vibrations of the beam coupled with an ordinary differential equation for the motion of the point-mass. The interest in such problems arises in transportation, especially in trains and trams traveling on rails, where the point-mass represents the motion of a wheel on the rail. Moreover, it may also represent a wheel traveling on a bridge or a crane with a moving load. The problem is of considerable interest, both theoretically and in applications. Theoretically, we established the existence of a weak solution to the problem using various tools from the theory of differential set-inclusions. Then, we studied the model computationally.

An improved algorithm for the problem was constructed in Section 4, and the results of its implementation presented in Section 5. Six different aspects of the problem were investigated numerically: (i) comparison of the dynamics of the Gao and the linear Euler–Bernoulli beams; (ii) the massless applied force and the load applied to a mass; (iii) a study of the dependence on p; (iv) the system behavior for different compressive tractions; (v) different velocities; and (vi) multiple passes of the mass over the span of the rail.

The comparison of the vibrations of the Gao beam and the linear Euler–Bernoulli beam shows the advantages of using the nonlinear Gao beam when the forces and the oscillations are not small. The comparison can be found in Fig. 5, in the massless case and in Fig. 6, in the inertial case ($m > 0$). In particular, the Euler–Bernoulli beam exhibited unreasonable and non-physical behavior, while the Gao beam produced reasonable vibrations. A study of the value of the critical compressive traction p^* above which the Gao beam buckles was conducted next, and the results depicted in Figs. 7 and 8.

The next set of simulations constituted one of the main results in this work. It studied the behavior of the system in six different scenarios with different values of the compressive horizontal traction, which was

the main novelty in the Gao beam model. The comparison among the results and also between the massless and the inertial cases can be found in Fig. 9. The results show clearly the increase in the frequency of the oscillations with increasing p, especially in the massless case. Moreover, the addition of a heavy mass was found to stabilize the system and to produce very well behaved vibrations. The vibrations of the system were found to be both interesting and important, in that in real wheel–rail systems the wheels may have considerable mass. Therefore, publication in the literature that do not include the case with mass may have led to incorrect conclusions.

A study of the reaction of the system to changes in the load velocity can be found in Figs. 10 and 11. It was seen that by increasing the load speed the oscillations decreased. We next investigated the system dynamics in successive transits of a single load, Fig. 12. The system's vibrations in the second pass where different since then the load started the pass on a vibrating beam, thus interacted with the vibrations created by its first pass. These results are of considered importance in applications when the second set of wheels of a tram or train passes on a rail that had been excited by the first set.

The final set of computer experiments dealt with the relationship between the system vibrations and the relative importance of the nonlinear Gao term in the equations of motion and the linear term with the compressive traction. It was found, Figs. 13 and 14, that when the traction at $x = 1$ was high, this term dominated and the system vibrations resembled more those of a string than those of the bending of a beam.

The numerical simulations indicated that describing the rail as a Gao beam seemed to be a better description if one is interested in the rail oscillations. One may notice that the influence of the Gao terms in the mathematical model is significant both mathematically and computationally. First, for beams with a low bending stiffness the Gao beam is much more rigid than the Euler–Bernoulli beam. Second, a soft Euler–Bernoulli beam is characteristic of lower eigenfrequency than a rigid one. In the case of the Gao beam this relation is reversed. Third, the higher external load increases the Gao beam features and strongly influences the frequency of the dynamic response. Still the range of parameters in real applications, for example in robotics, should be determined to evaluate the real difference between the Euler–Bernoulli and Gao models. The issue will have to be decided experimentally. We also note here that the vibrations of the system about a buckled states are novel, and cannot be studied by using any linear beam models.

Additional comments about the performance of the algorithm and the computations can be found at the end of Section 5.

Since the setting here is 'simple', we plan to continue this line of research and extend it in a number of directions. In this work we took into account the mass and its motion when the beam is buckled, while the issue of inclusion of thermal effects, which may be considerable if we allow for sliding and frictional heat generation, will be studied in the future. In such cases one must expand the system to allow for a horizontal friction traction and to add an equation for the thermal effects.

Acknowledgments

We thank the reviewer for the comments that considerably improved the presentation. This research has been supported within the projects UMO-2015/17/B/ST8/03244 and UMO-2017/26/E/ST8/00532 funded by the Polish National Science Centre, Poland, which is gratefully acknowledged by the authors.

Appendix

$$\mathbf{K}_n = \begin{bmatrix} -2(b^2(8q^2-3qs+s^2)+3b(p-r)(3s-4q)+12(p^2-2pr+r^2))/(35b^3) \\ -(b^2(3q^2-2qs+s^2)+12b(p-r)(s-q)+12(p^2-2pr+r^2))/(140b^2) \\ 2(b^2(q^2-3qs+8s^2)+3b(p-r)(3q-4s)+12(p^2-2pr+r^2))/(35b^3) \\ -(b^2(q^2-2qs+3s^2)+12b(p-r)(q-s)+12(p^2-2pr+r^2))/(140b^2) \end{bmatrix}$$

$$
\begin{bmatrix}
-(b^2(139q^2-50qs+25s^2)+12b(p-r)(17s-13q)+396(p^2-2pr+r^2))/(420b^2) & \\
(b^2(2q^2-qs+s^2)+3b(p-r)(3s-q)+18(p^2-2pr+r^2))/(105b) & \\
-(b^2(q^2+22qs-53s^2)+12b(p-r)(11s-q)+108(p^2-2pr+r^2))/(420b^2) & \\
(b^2(q^2+2qs-s^2)+24bs(p-r)+36(p^2-2pr+r^2))/(420b) &
\end{bmatrix}
\begin{bmatrix}
2(b^2(8q^2-3qs+s^2)+3b(p-r)(3s-4q)+12(p^2-2pr+r^2))/(35b^3) & \\
(b^2(3q^2-2qs+s^2)+12b(p-r)(s-q)+12(p^2-2pr+r^2))/(140b^2) & \\
-2(b^2(q^2-3qs+8s^2)+3b(p-r)(3q-4s)+12(p^2-2pr+r^2))/(35b^3) & \\
(b^2(q^2-2qs+3s^2)+12b(p-r)(q-s)+12(p^2-2pr+r^2))/(140b^2) &
\end{bmatrix}
\begin{bmatrix}
(b^2(53q^2-22qs-s^2)+12b(p-r)(s-11q)-108(p^2-2pr+r^2))/(420b^2) & \\
-(b^2(q^2-2qs-s^2)+24bq(r-p)-36(p^2-2pr+r^2))/(420b) & \\
(b^2(25q^2-50qs+139s^2)+12b(p-r)(17q-13s)+396(p^2-2pr+r^2))/(420b^2) & \\
-(b^2(q^2-qs+2s^2)+3b(p-r)(3q-s)+18(p^2-2pr+r^2))/(105b) &
\end{bmatrix},
$$

where

$$
\begin{aligned}
p &= \mathsf{w}_1 + (\alpha - 0.5\alpha^2)h\mathsf{v}_1 + 0.5\alpha^2 h\mathsf{v}_3\,,\\
q &= \psi_1 + (\alpha - 0.5\alpha^2)h\dot{\psi}_1 + 0.5\alpha^2 h\dot{\psi}_3\,,\\
r &= \mathsf{w}_2 + (\alpha - 0.5\alpha^2)h\mathsf{v}_2 + 0.5\alpha^2 h\mathsf{v}_4\,,\\
s &= \psi_2 + (\alpha - 0.5\alpha^2)h\dot{\psi}_2 + 0.5\alpha^2 h\dot{\psi}_4\,.
\end{aligned}
$$

References

[1] A.V. Metrikine, H.A. Dieterman, Instability of vibrations of a mass moving uniformly along an axially compressed beam on a viscoelastic foundation, J. Sound Vib. 201 (5) (1997) 567–576.

[2] Vladimir Stojanović, Predrag Kozić, Marko D. Petković, Dynamic instability and critical velocity of a mass moving uniformly along a stabilized infinity beam, Int. J. Solids Struct. 108 (2017) 164–174.

[3] Ping Xiang, H.P. Wang, L.Z. Jiang, Simulation and sensitivity analysis of microtubule-based biomechanical mass detector, J. Nanosci. Nanotechnol. 19 (2) (2019) 1018–1025.

[4] B. Dyniewicz, R. Konowrocki, C.I. Bajer, Intelligent adaptive control of the vehicle-span/track system, Mech. Syst. Signal Process. 53 (1) (2015) 1–14.

[5] D.Y. Gao, Nonlinear elastic beam theory with application in contact problems and variational approaches, Mech. Res. Commun. 23 (1) (1996) 11–17.

[6] M.F. M'Bengue, Analysis of a Nonlinear Dynamic Beam with Material Damage or Contact (Ph.D. thesis), Oakland University, 2008.

[7] K.L. Kuttler, J. Purcell, M. Shillor, Analysis and simulations of a contact problem for a nonlinear dynamic beam with a crack, Q. J. Mech. Appl. Math. (2011) http://dx.doi.org/10.1093/qjmam/hbr018.

[8] T. Dahlberg, Track issues, in: Simon Iwnicki (Ed.), Handbook of Railway Vehicle Dynamics, CRC Press, 2006, pp. 143–180.

[9] C.I. Bajer, R. Bogacz, Propagation of perturbances generated in classic track, and track with Y-type sleepers, Arch. Appl. Mech. 74 (2005) 754–761.

[10] C.I. Bajer, B. Dyniewicz, Numerical modelling of structure vibrations under inertial moving load, Arch. Appl. Mech. 79 (6–7) (2009) 499–508.

[11] J. Matej, A new mathematical model of the behaviour of a four-axle freight wagon with UIC single-link suspension, Proc. IMechE F: J. Rail Rapid Transit. 225 (6) (2011) 637–647.

[12] D.Y. Gao, D.L. Russell, An extended beam theory for smart materials applications: II. static formation problems, Appl. Math. Optim. 38 (1) (1998) 69–94.

[13] D.Y. Gao, Finite deformation beam models and triality theory in dynamical post-buckling analysis, Intl. J. Non-Linear Mech. 35 (2000) 103–131.

[14] D.L. Russell, L.W. White, A nonlinear elastic beam system with inelastic contact constraints, Appl. Math. Optim. 46 (2002) 291–312.

[15] K.T. Andrews, M.F. M'Bengue, M. Shillor, Vibrations of a nonlinear dynamic beam between two stops, Discrete Contin. Dyn. Syst. (DCDS-B) 12 (1) (2009) 23–38.

[16] M.F. M'Bengue, M. Shillor, Regularity result for the problem of vibrations of a nonlinear beam, Electron. J. Differential Equations 27 (2008) 1–12.

[17] K.T. Andrews, Y. Dumont, M.F. M'Bemgue, J. Purcell, M. Shillor, Analysis and simulations of a nonlinear dynamic beam, Appl. Math. Phys. (ZAMP) 63 (6) (2012) 1005–1019.
[18] J. Ahn, K.L. Kuttler, M. Shillor, Dynamic contact of two Gao beams, Electron. J. Differential Equations 194 (2012) 1–42.
[19] K.T. Andrews, K.L. Kuttler, M. Shillor, Dynamic Gao Beam in Contact with a Reactive or Rigid Foundation, Vol. 33, 2015, pp. 225–248.
[20] M. Shillor, M. Sofonea, J.J. Telega, Models and Analysis of Quasistatic Contact, in: Lecture Notes in Physics, 2004.
[21] K.L. Kuttler, M. Shillor, Set-valued pseudomonotone maps and degenerate evolution inclusions, Commun. Contemp. Math. 1 (1) (1999) 87–123.
[22] C.I. Bajer, B. Dyniewicz, M. Shillor, A Gao beam subjected to a moving inertial point load, Math. Mech. Solids 23 (3) (2018) 461–472, http://dx.doi.org/10.1177/1081286517718229.
[23] K.L. Kuttler, J. Li, M. Shillor, Existence for dynamic contact of a stochastic viscoelastic Gao beam, Nonlinear Anal. RWA 22 (4) (2015) 568–580.
[24] S. Migórski, A. Ochal, M. Sofonea, Nonlinear inclusions and hemivariational inequalities, in: Models and Analysis of Contact Problems, in: Advances in Mechanics and Mathematics, vol. 26, Springer, 2013.
[25] P. Wriggers, U. Nackenhorst (Eds.), Analysis and Simulation of Contact Problems, in: Lecture Notes in Applied and Computational Mechanics, vol. 27, Springer, 2006.
[26] M.E. Gurtin, Variational principles for linear initial–value problems, Quart. Appl. Math. 22 (1964) 252–256.
[27] I. Herrera, J. Bielak, A simplified version of Gurtin's variational principles, Arch. Ration. Mech. Anal. 53 (1974) 131–149.
[28] J.T. Oden, A generalized theory of finite elements. II. Applications, Internat. J. Numer. Methods Engrg. 1 (1969) 247–259.
[29] J.H. Argyris, A.S.L. Chan, Application of the finite elements in space and time, Ing. Archiv. 41 (1972) 235–257.
[30] C.I. Bajer, C. Bohatier, The soft way method and the velocity formulation, Comput. Struct. 55 (6) (1995) 1015–1025.
[31] B. Dyniewicz, D. Pisarski, C. Bajer, Vibrations of a Mindlin plate subjected to a pair of inertial loads moving in opposite directions, J. Sound Vib. 386 (2017) 265–282.
[32] C.I. Bajer, B. Dyniewicz, Virtual functions of the space–time finite element method in moving mass problems, Comput. Struct. 87 (2009) 444–455.
[33] B. Dyniewicz, Space–time finite element approach to general description of a moving inertial load, Finite Elem. Anal. Des. 62 (2012) 8–17.
[34] B. Dyniewicz, C.I. Bajer, Paradox of the particle's trajectory moving on a string, Arch. Appl. Mech. 79 (3) (2009) 213–223.
[35] B. Dyniewicz, C.I. Bajer, New feature of the solution of a Timoshenko beam carrying the moving mass particle, Arch. Mech. 62 (5) (2010) 327–341.